SECONDARY INJECTION LOCATION INFLUENCE ON DUAL-BELL NOZZLE TRANSITION BEHAVIOUR

Brian LEGROS*, Luc LEGER*†, Azeddine KOURTA‡, Amer CHPOUN[§], Mohamed SELLAM[§] and Virginie GILARD*

*National Centre for Scientific Research CNRS - Institute ICARE, Orleans, 45071, France

‡University of Orleans, INSA-CVL, PRISME, EA 4229, Orleans, 45100, France

§University of Evry, Paris-Saclay, Evry, 91020, France

brian.legros@cnrs-orleans.fr · †luc.leger@cnrs-orleans.fr

Abstract

This paper investigates the influence of the position of a transverse, annular secondary injection on the behaviour of a sub-scale dual-bell nozzle. Three dual-bell nozzles with different secondary injection slot positions in their extension profiles were tested under different secondary injection mass flow rate ratios and altitude conditions. The findings reveal that a secondary injection slot positioned upstream enables higher transition altitudes and stability with a lower secondary mass flow rate. However, above a critical secondary mass flow rate, the transition altitude decreases with an increase in secondary mass flow rate.

1. Introduction

The dual-bell nozzle (DBN) concept, initially introduced by Swan¹ in his investigation of step nozzles, consists of a converging/diverging nozzle, featuring a divergent section composed of two successive nozzle profiles with different expansion ratios. The two profiles are linked together through an inflection point. Its geometry is illustrated in Figure 1. This distinctive geometrical characteristic enables it to operate in two modes: a low-altitude mode, also known

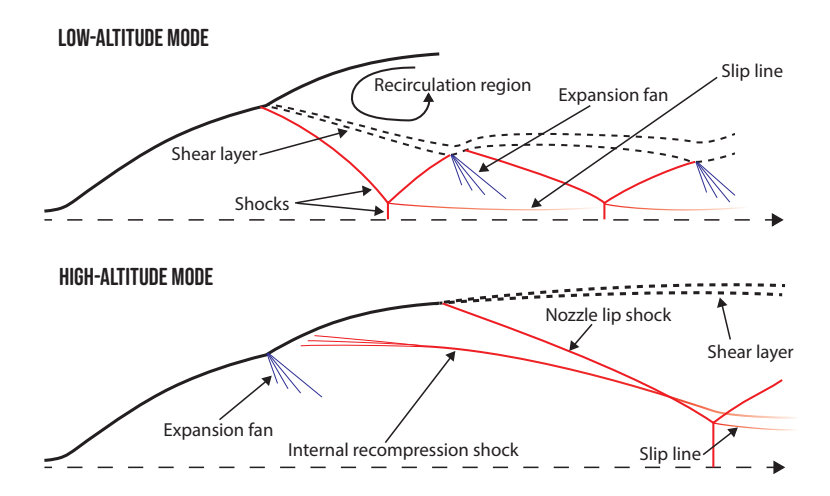


Figure 1: Operating modes in a dual-bell nozzle mounted with a constant pressure extension.

as sea-level mode, and a high-altitude mode. During sea-level mode, the flow is overexpanded and the high ambient pressure compresses the exhaust jet column. In this configuration, the boundary layer separates from the nozzle wall at the inflection point, providing a controlled and symmetric flow separation. It is noteworthy that the fixed position of the separation line at the inflection point plays a crucial role in reducing the risk of side-loads. Because the separation occurs at the base nozzle exit, the behaviour of the dual-bell nozzle is comparable to that of a conventional nozzle with an small expansion ratio. As the launcher ascends into the atmosphere, the ambient pressure decreases and the flow will eventually reattach the extension nozzle wall. During this process, known as transition, the flow expands through an expansion fan at the inflection point and the separation line moves from the inflection point to the nozzle exit. The increased expansion and the larger exit area naturally yield better performance at high altitudes. In the high-altitude

mode, the behaviour of the dual-bell nozzle is comparable to that of a conventional nozzle with a high expansion ratio. The switch from the low-altitude mode to the high-altitude mode is commonly referred to as the **transition**, and inversely, the switch from the high-altitude mode to the low-altitude mode is called the **retransition**. The behaviour of the dual-bell nozzle significantly varies depending on the contour design. The base nozzle and the extension nozzle may be designed independently, giving a wide range of dual-bell nozzle flow considerations. The base profile is often designed as an ideal contour. The expansion ratio is chosen for obtaining an overexpanded nozzle at sea-level. The ideal contour profile has the advantage of not inducing internal shock waves in the flow as is the case for optimised contours. At the base nozzle exit lies an inflection point. The greater the inflection angle α , the higher the transition nozzle pressure ratio (NPR, where $NPR = P_0/P_a$). The extension section plays the most important part in the dual-bell nozzle behaviour^{2,8} and three options are available for their design. The streamwise wall pressure either decreases, remains constant, or increases. In the literature, these three configurations are referred to as negative pressure gradient (NP), constant wall pressure (CP), and positive wall pressure gradient (PP) extensions. The CP and PP extension profiles provide an abrupt transition in which the separation line suddenly moves from the inflection point to the nozzle exit, limiting the risk of side-loads. However, in the NP extension profile occurs a continuous (no sudden) movement of the separation line throughout the nozzle driven by the change in nozzle pressure ratio, as observed in conventional bell nozzles. The substantial risk of high side-loads¹² associated with this gradual movement has reduced its appeal for industrial implementation and limited its academic investigation. The simplicity of the dual-bell nozzle concept represents a significant advancement that has the potential to reduce the cost of access to space for companies. However, despite its promise, several challenges must be addressed before considering the integration of dual-bell nozzles on rocket launchers. One of the scienfitic obstacle with the dual-bell nozzle is the early transition, characterised by the transition occurring before the optimum transition point, which results in significant losses (refer to Figure 2). The additional mass associated with the presence of an extension section needs to be compensated by optimal performance during the launches. This necessitates finding solutions to delay the natural early transition and to ensure efficient operation. The second great problem comes from the asymmetric separation line movement during the transition and retransition phases, which may induce high side-loads. Lastly, the presence of a small hysteresis (difference between the transition and retransition nozzle pressure ratios) could induce unstable swtiches between the low-altitude mode and the high-altitude mode.

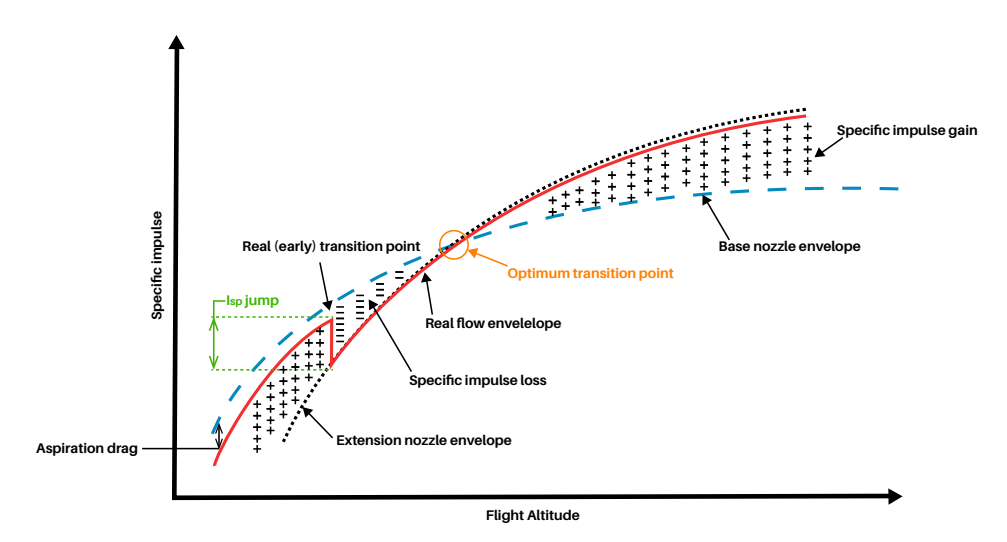


Figure 2: Schematic of the specific impulse as a function of flight altitude for conventional bell nozzles and the dual-bell nozzle.⁶

Most research tackling the dual-bell nozzle's scientific obstacles dealt with flow control through the injection of a secondary gas in the vicinity of the inflection point. Two main methods have been employed: secondary injection parallel to the mainstream, commonly used for film cooling, and secondary injection in the perpendicular direction of the mainstream flow. The film cooling technique has shown limited impact on addressing the three major challenges faced by dual-bell nozzles: early transition, side-loads, and stability. A 2009 study observed the potential to lower wall temperatures but at the expense of enduring lateral forces. Numerical simulations indicated a decrease in transition nozzle pressure ratio with varying mixture ratios and secondary injection mass flow rates. Conversely, the transition nozzle pressure ratio increased with operating film cooling in another study. The latter study also reported a reduction in thrust jump during transition phases and lower side-loads.

Annular, radial fluidic secondary injection has been the subject of past investigations. Tomita et al. (2009) conducted

a cold flow test on a dual-bell nozzle equipped with a PP extension operating with secondary injection at the inflection point.¹³ The experiment revealed that secondary injection decreased the transition nozzle pressure ratio, thereby increasing the gap toward the optimum transition point.

The latest experimental test campaigns, conducted at the ICARE Institute of CNRS on a dual-bell nozzle equipped with a CP extension, demonstrated a notable and positive impact of secondary injection on a subscale dual-bell nozzle's behaviour when the injection was positioned downstream of the inflection point (in the extension section).^{3,6,15} In this case, the transition nozzle pressure ratio was increased, and side-loads were reduced during changes in operating modes. The positive effect of secondary injection was distinctly observed, even for relatively modest secondary-to-primary mass flow rates (less than 1%). The experiments also indicated the influence of secondary injection on the dual-bell nozzle's stability with a modified hysteresis.⁴

These preliminary studies demonstrated the possibility of improving a dual-bell nozzle's performance by employing annular, radial secondary injection downstream of the inflection point. However, optimisation of the control method, considering factors such as secondary injection pressure, injection location, or injectant gas, is still lacking. Therefore, the present study aims to provide a more thorough investigation of this control method by exploring the influence of the secondary injection location on the behaviour of a sub-scale dual-bell nozzle.

2. Experimental setup

Four subscale dual-bell nozzles were manufactured to perform the investigations: a reference dual-bell nozzle (without a secondary injection slot), and three dual-bell nozzles with a secondary injection slot located 4 mm, 8 mm, and 16 mm downstream of the inflection point. These three nozzles are referred to as DBNi4, DBNi8, and DBNi16, respectively. The reference nozzle was designed using the method of characteristics. The base nozzle was designed as an ideal contour for an exit Mach number of three and was truncated at a wall Mach number of 2.76. The extension nozzle was built as a constant pressure extension profile for an exit Mach number of 3.17 after the 8 degrees expansion at the inflection point. The transition nozzle pressure ratio estimated from the Stark criterion⁹ amounted to 14.89. The nozzles integrating a secondary injection slot possess an identical wall profile as the reference nozzle. The presence of the secondary injection slot was made possible by designing the dual-bell nozzles in two separate parts: the first part contains the nozzle profile from the convergent inlet to the upstream edge of the secondary injection slot, while the second part extends from the downstream edge of secondary injection slot to the nozzle exit. To make room for a 0.2 mm annular injection width, 0.2 mm of material was removed from the upstream end of the second part, allowing for the slot to form upon assembly of the two sections (see Figure 3). This two-part design also enables the incorporation of a secondary injection settling chamber to set the stagnation conditions for the secondary injection flow. This secondary injection settling chamber is referred to as the cavity throughout this paper. The cavity and the annular secondary injection slot presence provided an axisymmetric, homogeneous secondary injection. The dual-bell nozzles' parameters are summarised in Table 1. Air is used as the working fluid for both the main and secondary flows. The experimental test campaigns were conducted at the FAST (Facilities for Aerothermodynamics and Supersonic

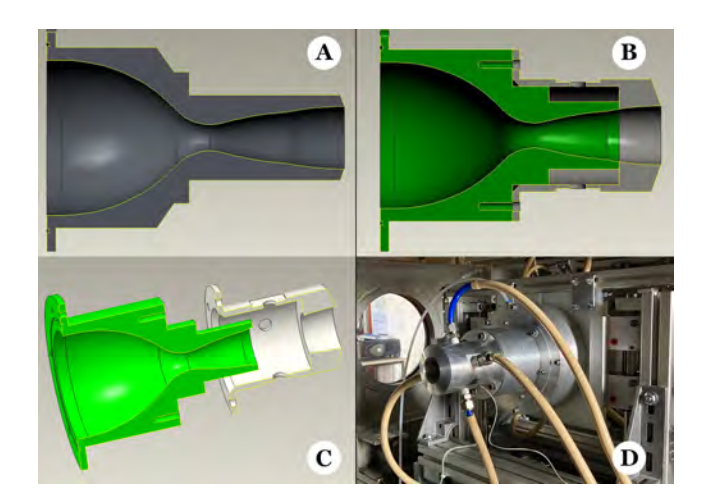


Figure 3: A) Reference dual-bell nozzle), B) DBNi8, C) Exploded view of DBNi8, D) DBNi8 mounted with secondary injection pipes in the EDITH wind tunnel.

Technologies) platform of the ICARE Institute of CNRS. The experiments were performed in the EDITH wind tunnel, a blow-down type wind tunnel offering nozzle test measurements in a depressurised environment. Dry air from 320

Table 1: Dual-bell nozzle parameters

Parameter	Value
Throat radius	$r_{th} = 0.0085 \text{ m}$
Base nozzle geometry	Length: $l_b/r_{th} = 5.89$
	Expansion ratio: $\epsilon_b = 3.78$
Extension nozzle geometry	Length: $l_e/r_{th} = 4.32$
	Expansion ratio: $\epsilon_e = 5.67$
Inflection angle	$\alpha = 8 \deg$
Injection slot	Width: $d_i/r_{th} = 0.024$
	Location: $\{0.47,0.94;1.88\}r_{th}$ downstream inflection
Design transition nozzle pressure ratio (Stark's criterion ⁹)	$NPR_{trans} = 14.89$

litre tanks and pressurized at 30,000 kPa is regulated to 350 kPa to serve as the nozzle feeding total pressure. The flow is injected in the nozzle convergent inlet through six 10-mm-diameter radially distributed pipes. Then, the air travels through the dual-bell nozzle and exits in the depressurised facility test section. The pressure inside the test section is controlled by a butterfly-type valve upstream of an overall 345 kW power pumping group in the test facility diffuser. Further details regarding the test facility are provided in previous investigations.^{6,15}

During the experiments, the mainstream feeding total pressure is kept constant. In contrast, the ambient pressure in the facility test section is repetitively increased and decreased between a nozzle pressure ratio of ≈ 11.67 and \approx 60 to trigger the transition and retransition phases. For experiments involving active flow control with transverse secondary injection, the cavity is fed from a secondary pressure line connected to the 600 kPa laboratory compressed air reservoir. Before entering the cavity, the secondary feeding pressure is regulated, and the flow is split into four secondary injection pipes connected symmetrically to the cavity's outer wall (see Figure 3). When secondary injection is active, its pressure is kept constant throughout the experiment. The stagnation pressure P_i used to feed the secondary jet averagely ranged within $P_i \in [24.3;217.1]$ kPa, depending on the nozzle under investigation. More details regarding the secondary injection are available in Table 2. The dual-bell mainstream stagnation pressure was measured using an



Figure 4: Experimental facility.

Omega 100 to 700 kPa range pressure transducer. When a nozzle with a secondary injection slot was operated (with or without secondary injection), the stagnation pressure inside the cavity was measured using a Kulite XCQ-062 pressure transducer with a range of 0-100 kPa. For secondary injection pressures above 88 kPa, the pressure transducer inside the cavity was replaced by a Kulite XCQ-093 with a 0-350 kPa range. The ambient pressure in the wind tunnel test section was measured using a Kulite XCQ-062 pressure transducer with a 0-100 kPa range. The dual-bell nozzle is mounted on a force balance designed by the authors and reported in previous studies.¹⁴ It measures the thrust and lateral forces using four HBM S2 strain-gauge force transducers. The transducers' signals are amplified to a 0-10 V range by an HBM RM4220 amplifier before being acquired by the SCXI-1140 cards at 1000 Hz. Two transducers of a nominal range of 0-200 N located on both sides of the force balance were used to measure the vertical force

Table 2: Secondary injection pressure, pressure ratio (SPR), mass flow rate (\dot{m}_i), and mass flow rate ratio ($\varphi_{\dot{m}}$) used in test campaign.

DBNi4								
Pressure [kPa]	0	24.3	52.8	67.7	113.1	152.1	191.9	-
SPR	0	0.07	0.15	0.19	0.32	0.44	0.55	-
\dot{m}_i , [g/s]	0	1.25	2.72	3.49	5.83	7.84	9.90	-
$arphi_{\dot{m}}$	0	0.007	0.015	0.019	0.031	0.042	0.053	-
DBNi8								
Pressure [kPa]	0	36.9	50.9	69.1	88.0	125.7	163.4	217.1
SPR	0	0.11	0.15	0.2	0.25	0.36	0.47	0.62
\dot{m}_i , [g/s]	0	1.98	2.73	3.70	4.72	6.73	8.75	11.63
$arphi_{\dot{m}}$	0	0.011	0.015	0.020	0.025	0.036	0.047	0.062
DBNi16								
Pressure [kPa]	0	36.6	50.7	65.3	87.8	-	-	-
SPR	0	0.11	0.15	0.19	0.25	-	-	-
\dot{m}_i , [g/s]	0	2.07	2.87	3.70	4.97	-	-	-
$arphi_{\dot{m}}$	0	0.011	0.015	0.020	0.027	-	-	-

component; one 0-200 N range transducer measured the nozzle thrust; and a 0-20 N transducer measured the lateral forces. Previous studies for the validation of the force balance measurements showed a 0.24 N standard deviation for the force measurements on the longitudinal axis, 0.06 N on the vertical axis and 0.17 N on the lateral axis. For dual-bell nozzles tests in the current operating conditions, the 300-bars, 320 litres high-pressure tanks allows for five to seven cycles during one experiment. Each experiment is repeated twice to have between 10 to 14 transitions and retransitions, allowing for the presentation of curves with representative error bars.

2.1 Configuration for the reference nozzle, DBNi8, and DBNi16 test specimen

All measured quantities were recorded at a frequency of 1000 Hz. The nozzle flow visualization was made possible via the z-schlieren system described in previous work³ and a Canon®EOS60D camera, recording images at a frequency of 50 Hz.

2.2 Configuration for the DBNi4 test specimen

As the wind tunnel is undergoing equipment update, the experimental setup for the DBNi4 test specimen differed slightly. In this case, the acquisition system had changed from the National Instruments SCXI-1140 to a HIOKI MR6000, and all measured quantities were recorded at 10 kHz. The Canon® EOS60D camera was also replaced by a i-SPEED® 5 series 509-S high-speed camera, recording images at 50 Hz in the present test campaign.

3. Results and Discussions

Figure 5 shows the, specific impulse, nozzle pressure ratio, secondary mass flow rate ratio, and side-loads ratio as a function of time during a customary experiment in DBNi4. The side-loads ratio is computed as the magnitude of the side-loads divided by the thrust. When the nozzle pressure is at its lowest (NPR~11), the dual-bell nozzle operates in the low-altitude mode. Then, the pressure inside the wind tunnel test section is decreased, causing a rise in nozzle pressure ratio. When the transition nozzle pressure is reached, the dual-bell switches from the low-altitude mode to the high-altitude mode. After the transition to high-altitude mode, the pressure inside the wind tunnel continues to decrease until a maximum of nozzle pressure ratio. Following this maximum, the ambient pressure is increased, causing the nozzle pressure ratio to decrease. When the retransition nozzle pressure is reached, the dual-bell switches from the high-altitude mode to the low-altitude mode. The ambient pressure continues to increase until a minimum value of nozzle pressure ratio, after which the ambient pressure rises again to trigger the transition, and so on for as long as the stagnation conditions can be maintained. During these cycles, the following parameters are measured to characterise the influence of secondary injection on the dual-bell nozzle: transition and retransition nozzle pressure

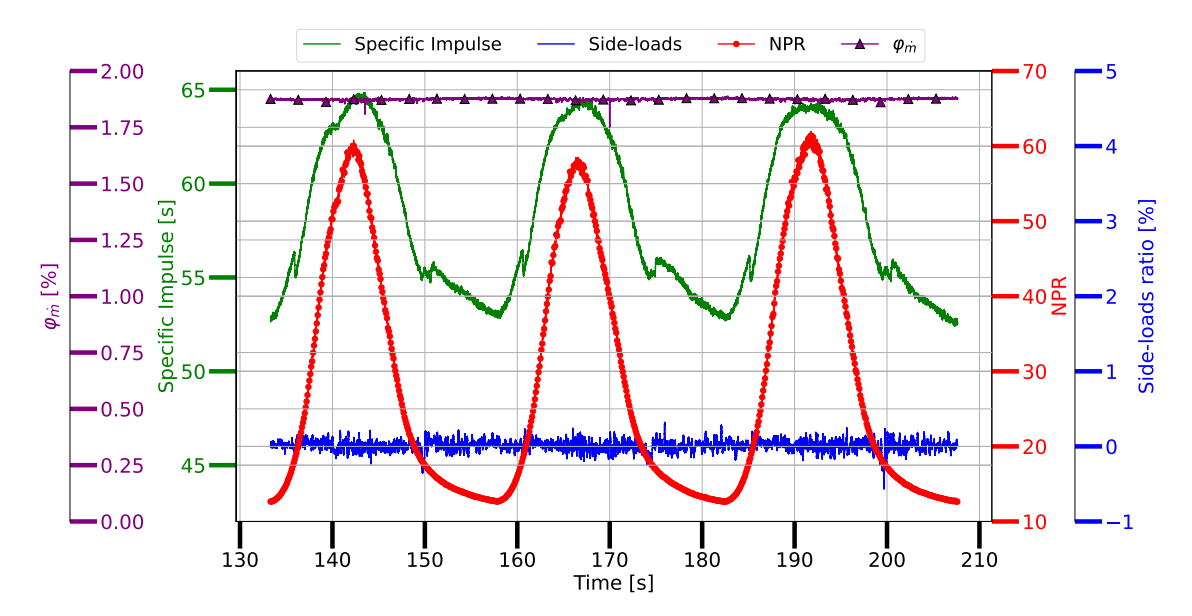


Figure 5: Specific impulse, nozzle pressure ratio (NPR), secondary mass flow rate ratio (φ_m), and side-loads ratio as a function of time: DBNi4 operating with $\varphi_m \approx 0.019$.

ratios, thrust, side loads, and thrust drop (respectively rise) during the transitions (respectively retransitions). Figure 6 displays the specific impulse as a function of nozzle pressure ratio during a transition and a retransition phase for DBNi4. The sudden transition and retransition are easily noticeable.

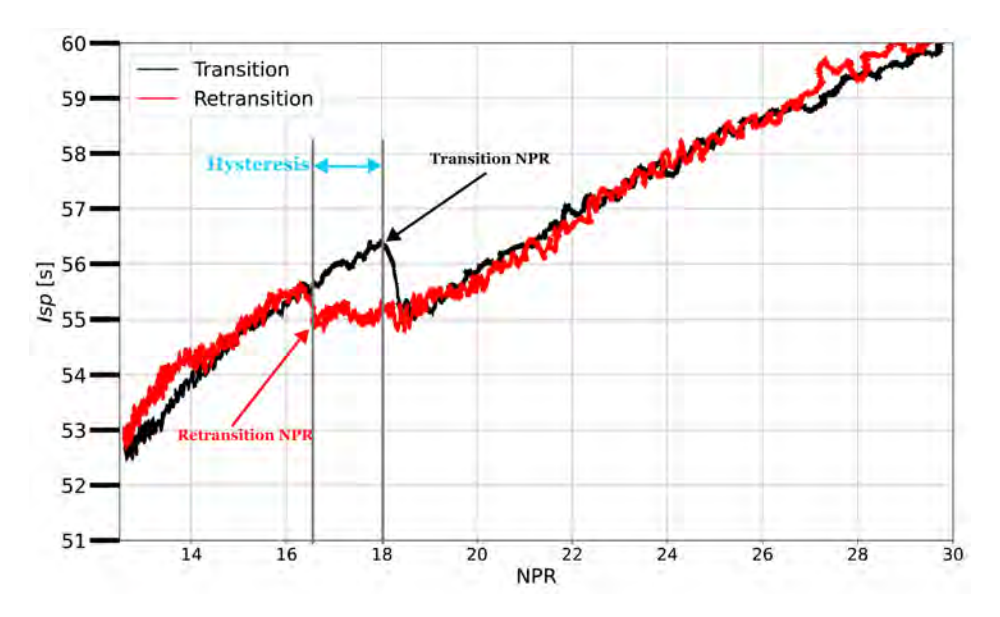


Figure 6: Specific impulse as a function of nozzle pressure ratio during a transition phase and a retransition phase for DBNi4 operating with $\varphi_m \approx 0.019$.

Figure 6 also exhibit the hysteresis effect present in this type of nozzle, where the transition and retransition nozzle pressure ratios are different. The hysteresis, generally computed as in Eq. 1, is a indicator of the dual-bell nozzle stability. A dual-bell nozzle characterised by a little hysteresis is more likely to suffer from uncontrollable switches between the low-altitude mode and the high-altitude mode (often called flip-flop) under significant ambient pressure fluctuations than one with a large hysteresis.

$$Hysteresis = \frac{NPR_{trans} - NPR_{retrans}}{NPR_{trans}} * 100$$
 (1)

Before diving into a comprehensive comparison, it is interesting to see that the location of the secondary injection may dramatically influence the transition and retransition behaviour of the nozzle. Figure 7 shows the specific impulse

as a function of nozzle pressure ratio during an ascent phase for all dual-bell nozzles. The constant wall pressure chosen for the extension profile assures, theoretically, rapid transitions and retransitions. These rapid operating mode switches are observable in the reference dual-bell nozzle, DBNi4, and DBNi8. However, as the injection slot is moved further downstream for the DBNi16 test specimen, the transitions and retransitions occur continuously, with no sudden rise, or drop, of specific impulse. This behaviour appears when the secondary mass flow rate ratio becomes larger than 0.011. The authors suspect that performing secondary injection further downstream allows the separation front to progressively move between the inflection point and the nozzle exit when the nozzle pressure ratio is varied. However, further investigation is necessary to fully identify the mechanisms responsible for this change of behaviour.

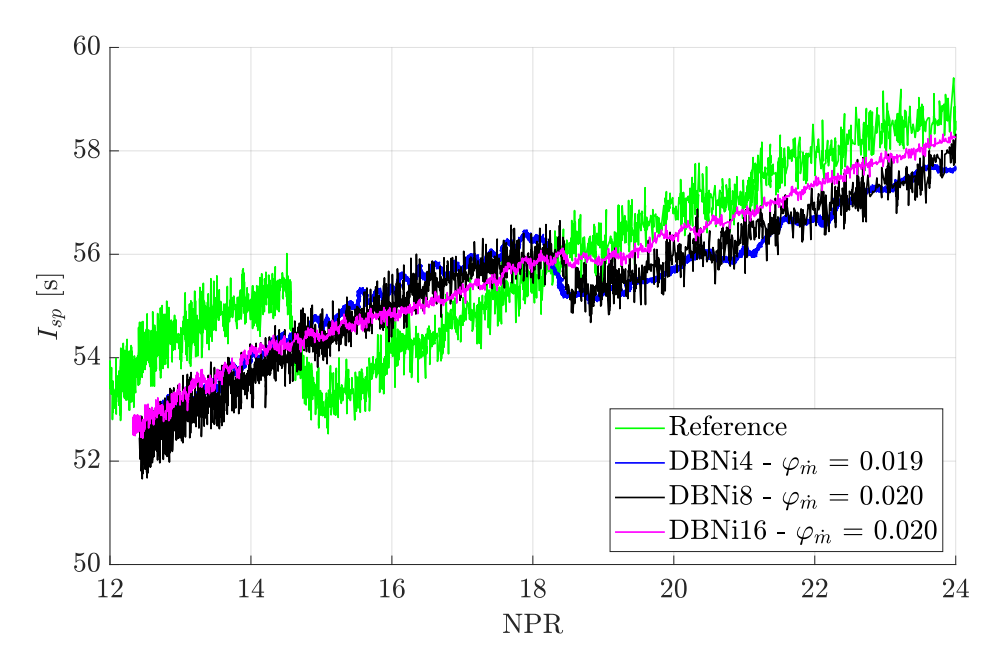


Figure 7: Specific impulse as a function of nozzle pressure ratio during a transition phase for the reference dual-bell nozzle and the other test specimen operating with $\varphi_m \approx 0.020$.

3.1 Qualitative analysis

This section compares a series of schlieren images from the experiments performed with the DBNi8 and DBNi16 test specimens. The DBNi4 configuration was not shown here as the shock topologies remain relatively similar to those observed in the other test specimen. Also, the shock system being similar during the ascent and descent phases, the exhaust flow features are discussed for several nozzle pressure ratios during the transition phase only. Figure 8 shows Schlieren images of the dual-bell nozzle exhaust plume for roughly NPR \in [17.4;50] in the DBNi8 and DBNi16 nozzles operating at $\varphi_m = 0.025$ and $\varphi_m = 0.027$, respectively.

At NPR \approx 17.4, the two dual-bell nozzles operate in low-altitude mode and the shock system inside the nozzles is not visible. Here, the secondary jet acts as an obstacle and generates a bow shock wave locally. The adverse pressure gradient induced by the jet causes the boundary layer to separate upstream, inducing an oblique separation shock. Downstream, another shock is formed from the core flow compression by the high ambient pressure. Reflections of these two shock structures are visible in Figure 8a. The proximity between these two structures in the DBNi16 test specimen makes it more challenging to distinguish between them, especially since the internal flow visualisation is not available. For both test specimens, a series of compression and expansion cells follow these structures until the exhaust plume pressure adapts to the ambient pressure in the wind tunnel test section.

As the nozzle pressure ratio increases to 18, the flow expands, and the two principal shock structures move downstream for both dual-bell nozzles. However, the two shocks remain difficult to tell apart in the DBNi16 configuration.

At a nozzle pressure ratio of \sim 18.50, the transition from the low-altitude mode to the high-altitude mode occurred almost fully in the DBNi8 test specimen. Here, the flow has reattached to the extension section wall, but the absence of an internal recompression shock suggests that the flow is not fully attached to the entirety of the extension wall. Similarly to the low-altitude mode, the higher ambient pressure compresses the jet column and an oblique shock wave emerges from the nozzle wall. At this nozzle pressure ratio, the strong nature of the shock induced by high ambient pressure is supported by the singular Mach reflection in the Schlieren images, along with a reflected shock and slip

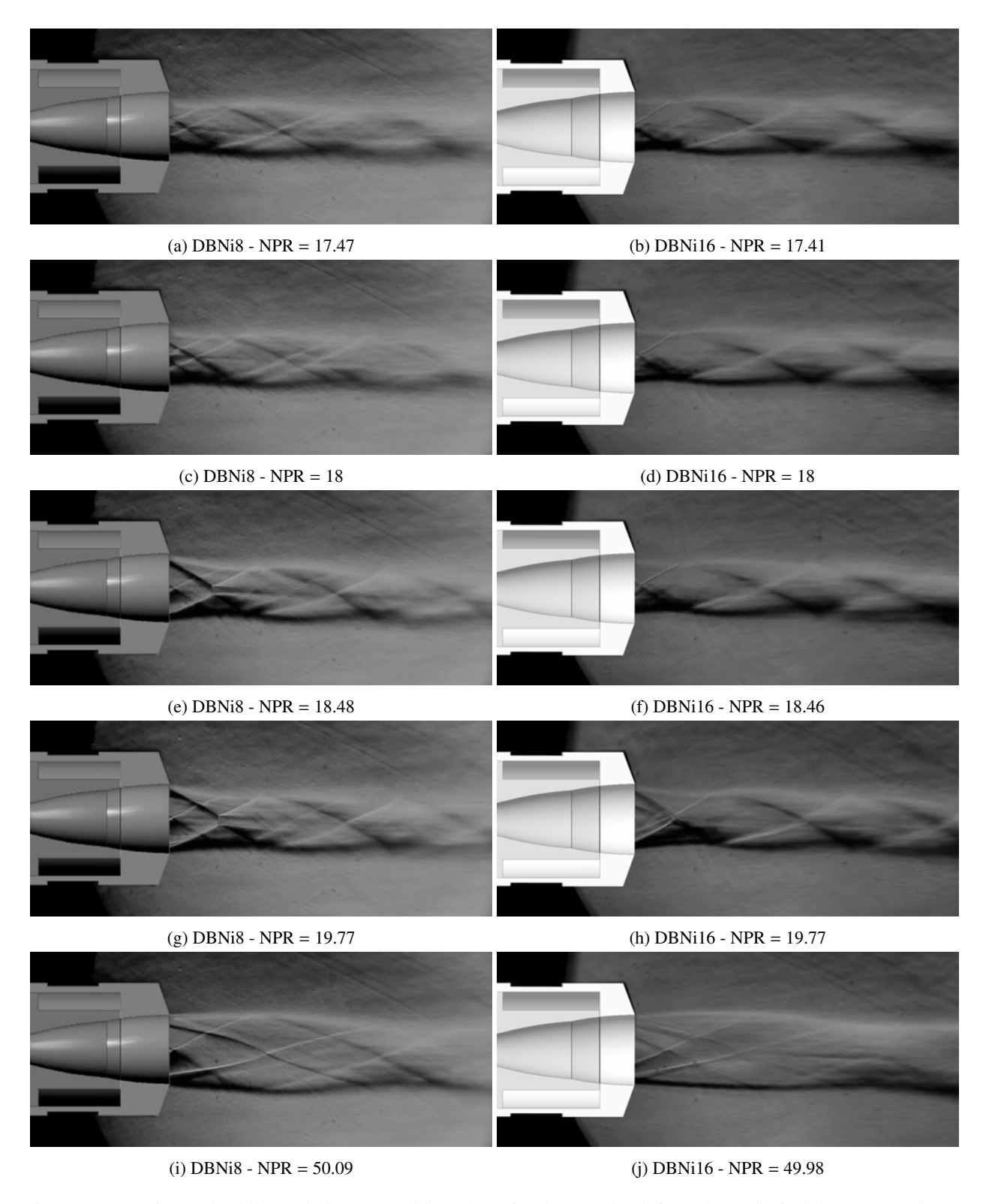


Figure 8: Experimental schlieren during a transition phase for the DBNi8 (left) and DBNi16 (right) test specimens operating at $\varphi_m = 0.025$ and $\varphi_m = 0.027$, respectively.

lines at the triple point. Both, the shock induced by the secondary injection and the shock caused by the high ambient pressure induce a series of compression and expansion cells in the exhaust plume downstream. Conversely, the DBNi16 has yet to transition to the high-altitude mode and the shock system is the same as for NPR = 18.

At a nozzle pressure ratio of 19.77, the transition has taken place in the DBNi16 nozzle. The shock induced by the

secondary injection, the oblique shock induced by the high ambient pressure, and the Mach disk become apparent. Similarly to the DBNi8 nozzle at NPR = 18.48, the DBNi16 does not show any internal recompression shock, which suggests that the flow is not fully attached to the entirety of the extension wall. The well-known compression and expansion cells following the primary shock systems are also visible. As for the DBNi8 nozzle, the transition has fully occurred, and an internal recompression shock becomes apparent due to the constant pressure nature of the extension section.

At NPR \approx 50, the two DBNs operate in the high-altitude mode. The oblique shock induced by the ambient pressure ceased to exist. Both schlieren images display the shock induced by the secondary injection and the internal recompression shock, which extends throughout the exhaust plume. Because the secondary injection slot is displaced in the aft part of the extension section in the DBNi16 nozzle, the reflection of the shock induced by the secondary injection is displaced further downstream, as opposed to the DBNi8 test specimen, where the reflection is positioned in the vicinity of the nozzle exit. Nonetheless, both shock topologies exhibit similar patterns.

It is noteworthy to mention that, in the experiments conducted in the DBNi16 with relatively high secondary mass flow rate ratios, the Schlieren videos revealed transition and retransition phases that appeared to unfold more continuously, with less abruptness. The subsequent section studies more quantitaviely the effects of the position of secondary injection on the behaviour of the dual-bell nozzle.

3.2 Quantitative analysis

Previous studies experimentally demonstrated the capability of transverse, annular secondary injection to increase the transition and retransition nozzle pressure ratios when the secondary mass flow rate ratio is increased.⁶ The study also showed the limitations of the control method as the authors observed a decrease in transition and retransition nozzle pressure ratio when the secondary mass flow rate ratio increased further than 0.025 and 0.036, respectively. Figure 9 shows the transition nozzle pressure ratio measured in DBNi4, DBNi8, and DBNi16 for several secondary mass flow rate ratios. The experimental measurements obtained in a previous study⁶ are represented by the black squares.

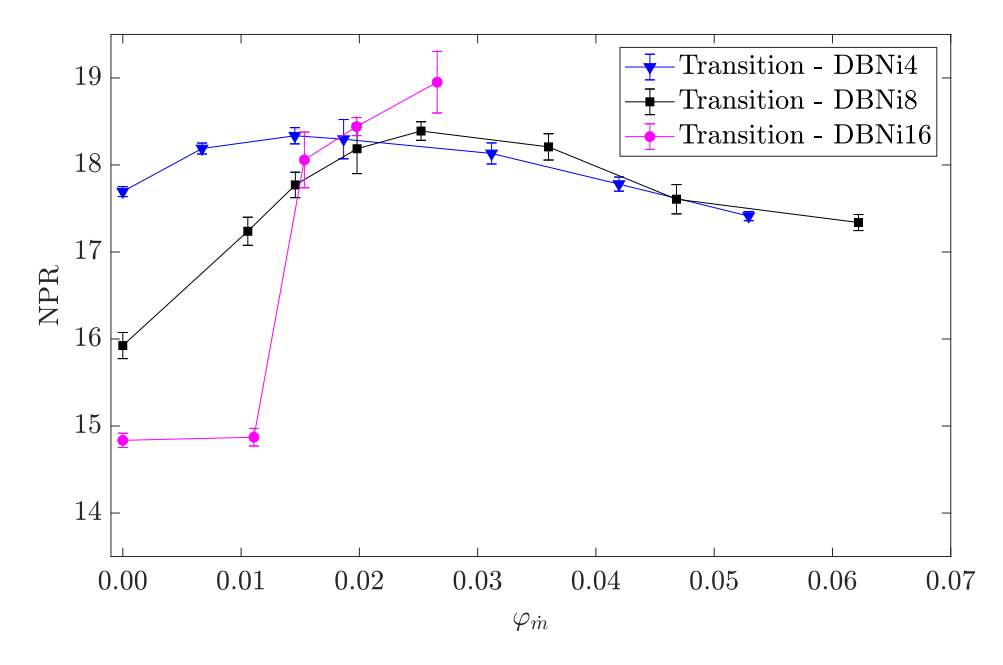


Figure 9: Transition nozzle pressure ratio as a function of secondary mass flow rate ratio for different secondary injection positions.

The figure clearly reveals that the transition nozzle pressure ratio is appreciably influenced by the secondary injection slot location. Actually, the mere presence of the injection slot, without applying a secondary injection pressure, is sufficient to affect the transition nozzle pressure ratio. When no secondary injection is applied, i.e. $\varphi_m=0$, the experimental measurements clearly shows that the closer the secondary injection slot to the inflection point, the larger the transition nozzle pressure ratio. In these conditions, a transition nozzle pressure ratio of 14.84 was measured for DBNi16 test specimen. When compared to the reference dual-bell nozzle, this corresponds to a decrease of 0.07%, suggesting that the furthest secondary injection slot has almost no influence on the dual-bell nozzle transition behaviour when no secondary injection pressure is applied. Meanwhile, for the same configuration, i.e. $\varphi_m=0$, the DBNi4 and

DBNi8 test specimen exhibited transition nozzle pressure ratios of 17.69 and 15.92, corresponding to an increase of 19.2% and 7.3% when compared to the reference dual-bell nozzle, respectively. When the secondary injection pressure is employed, a trend similar to the one of the previous study⁶ is observed, namely the increase in transition nozzle pressure ratio with an increase in secondary mass flow rate ratio. The increase in transition nozzle pressure ratio is also found to be limited in the DBNi4 test specimen, as it was observed for the DBNi8 test specimen.⁶ Furthermore, the experiments show that the extent of this increase and the secondary mass flow rate ratio at which the maximum increase occurs depend of the secondary injection slot location. Compared to their respective configuration where no secondary injection is applied, the transition nozzle pressure ratio increases by up to 3.6% and 15.5% for the DBNi4 and the DBNi8 test specimen, bringing their maximum transition nozzle pressure to 18.34 and 18.39, respectively. When compared to the reference nozzle, the latter correspond to a increase of 23.5% and 23.9%, respectively. The maximum transition nozzle pressure ratio occurs for a secondary mass flow rate ratio of 0.015 and 0.025 for the DBNi4 and DBNi8 test specimen, respectively. If the secondary mass flow rate ratio increases further than the aforementioned values, a decrease in transition nozzle pressure ratio is observed. The maximum decrease was up to 5% and 5.7% for the DBNi4 and DBNi8 test specimen when compared to their maximum transition nozzle pressure ratio. Steady-state Reynolds-Averaged Navier-Stokes simulations carried out internally suggest that this decrease occurs when the boundary layer separation line is pushed upstream of the inflection point by the secondary injection jet. Since a secondary injection slot positioned closer to the inflection point allows the boundary layer to separate upstream of the inflection point with a lower secondary mass flow rate ratio than a downstream position, the maximum transition nozzle pressure ratio is achieved with a smaller secondary mass flow rate in the former configuration-consistent with experimental observations. It is worth highlighting that the experimental data measured in the DBNi16 test specimen for secondary mass flow rate ratios higher than 0.025 is not displayed. This is due to the continuous transition observed in this dualbell nozzle, which would not allow the authors to clearly identify the transition nozzle pressure ratios. Nevertheless, Figure 9 shows that a secondary mass flow rate ratio larger than 0.011 is necessary for the secondary injection to begin influencing the transition nozzle pressure ratio in the DBNi16 test specimen. Below this value, operating secondary injection in the extension has almost no influence on the dual-bell nozzle transition behaviour. Above this value and until a secondary mass flow rate ratio of 0.027, the transition nozzle pressure ratios are in the vicinity of the ones measured in the other test specimen, at the exception that a more continuous transition occurs as the secondary jet pressure is increased.

During the retransition phase, the dual-bell nozzle switches from the high-altitude mode, where the flow is attached to the extension section, to the low-altitude mode, where the flow separates from the nozzle wall at the inflection point and does not reattach the extension wall. Figure 10 shows the retransition nozzle pressure ratio measured in DBNi4, DBNi8, and DBNi16 for several secondary mass flow rate ratios.

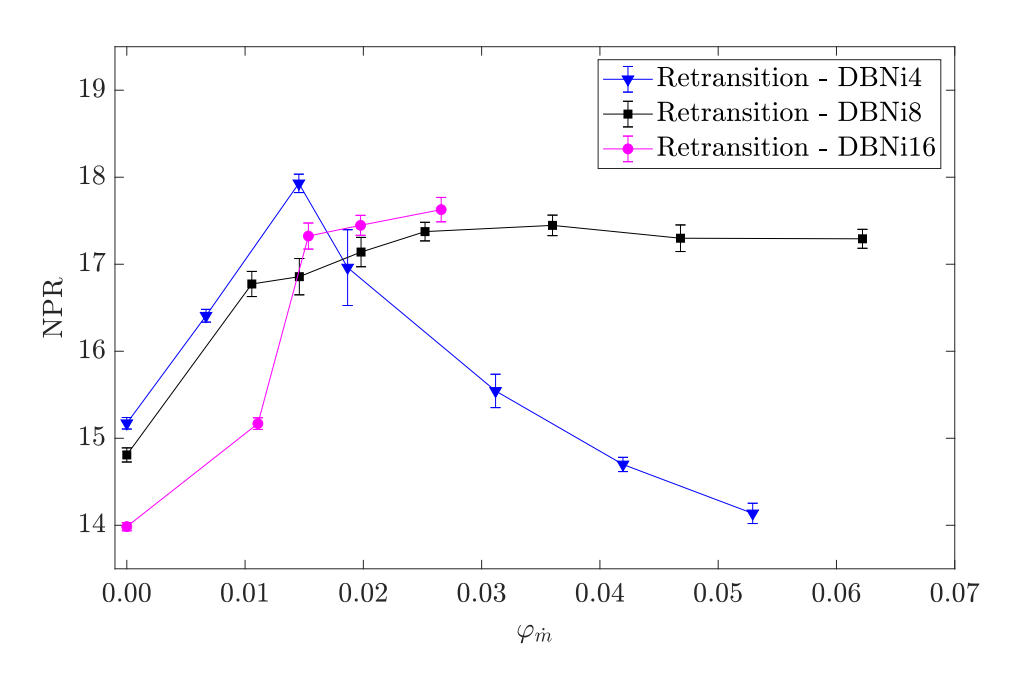


Figure 10: Retransition nozzle pressure ratio as a function of secondary mass flow rate ratio for different secondary injection positions.

The experimental measurements obtained in the previous study⁶ are represented by the black squares. It reveals that in

the absence of secondary injection pressure, a downstream displacement of the secondary injection induces a decrease in retransition nozzle pressure ratio, with measured values of 15.17, 14.81, and 13.98 for the DBNi4, DBNi8, and DBNi16, respectively. The latter correspond to an increase of 4.5% and 1.9% for the DBNi4 and DBNi8 test specimen when compared to the reference nozzle, but a decrease for 3.7% for the DBNi16 nozzle. The experimental data also show that the retransition nozzle pressure increases with the secondary mass flow rate ratio. The latter is true for 1) the DBNi4 test specimen for secondary mass flow rate ratios between 0 and 0.015, 2) the DBNi8 test specimen for secondary mass flow rate ratios between 0 and 0.036, and 3) the DBNi16 test specimen for secondary mass flow rate ratios between 0 and 0.027. In the aforementioned ranges, the rise in secondary mass flow rate ratio increases the secondary jet obstacle in the upcoming attached flow. The larger obstacles increase the severity of the adverse conditions in the extension section. Consequently, increasing the secondary mass flow rate ratio causes the initially attached flow to separate from the extension wall earlier, i.e. at larger nozzle pressure ratios, hence the higher retransition nozzle pressure ratio. When the secondary mass flow rate ratios exceed the aforementioned ranges, the experiments show that the retransition nozzle pressure ratio decrease when the secondary mass flow rate ratio increases. The behaviour, firstly identified in a recent paper, 6 is now confirmed in the present investigation, especially in the DBNi4 test specimen. However, the present study shows the influence of the secondary injection slot location on the extent of this phenomenon. In the DBNi8 test specimen for the secondary mass flow rate ratios investigated, the retransition nozzle pressure ratio decreased by up to 0.9% from its maximum value. Meanwhile, in the DBNi4 test specimen, the retransition decreased by up to 21.2%. In the DBNi4 test specimen, the closer proximity of secondary jet with the inflection point not only seems to intensify the extent of this decrease, but it also causes the maximum retransition nozzle pressure ratio to be reached for a lower secondary mass flow rate ratio. In both cases and similarly to the transition phase described above, the decrease in retransition nozzle pressure ratio is suspected to emanate from the different nature of interaction between the separation line caused by the presence of the secondary injection jet and the inflection point. Nevertheless, further investigation is necessary to fully understand the mechanisms present in this newly observed phenomenon. Note that, as explained in the previous paragraph on the transition nozzle pressure ratio analysis, experiments using the DBNi16 test specimen for secondary mass flow rate ratios higher than 0.025 were not carried out due to the continuous transition observed in this dual-bell nozzle.

The hysteresis, given by Eq. 1 is an important parameter as it is a criterion for the dual-bell nozzle stability. The larger the hysteresis, the less likely the dual-bell nozzle is to suffer from the flip-flop phenomenon.

Figure 11 displays the dual-bell nozzle hysteresis as a function of secondary mass flow rate ratio for the different test specimen.

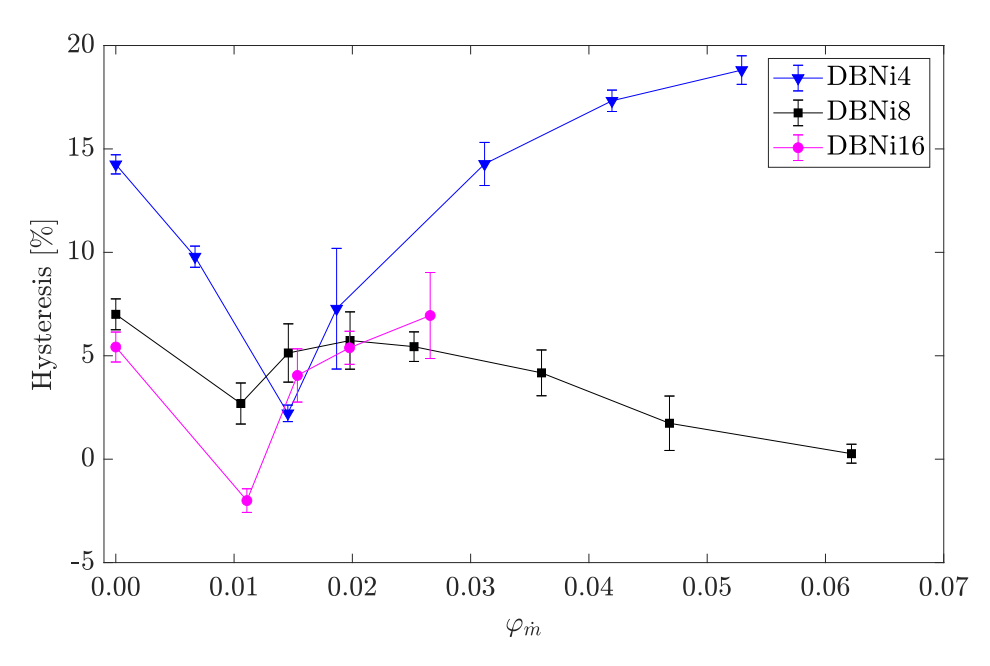


Figure 11: Dual-bell nozzle hysteresis as a function of secondary mass flow rate ratio for different secondary injection positions.

It shows that the hysteresis depends on the secondary injection slot location. In the absence of secondary injection, the DBNi4, DBNi8, and DBNi16 test specimen display a hysteresis of 14.3%, 7%, and 5.4%. The significant hysteresis achieved by the DBNi4 test specimen is mostly associated with its larger transition nozzle pressure ratio while having

a retransition nozzle pressure ratio in the vicinity of that of the other test specimen. The DBNi4 test specimen also provides the largest hysteresis, with 18.8% for a secondary mass flow rate ratio of 0.053. The significant hysteresis growth observed for the DBNi4 test specimen emanates from the substancial drop in retransition nozzle pressure ratio when the secondary mass flow rate ratio increases. The figure also shows that for all configurations, the hysteresis decreases with an increase in secondary mass flow rate ratio until a critical value at which a local minimum of hysteresis is reached. The hysteresis measured at the critical point amounted to 2.2%, 2.7%, and -2% for the DBNi4, DBNi8, and DBNi16 test specimen, respectively. In the latter configuration, the negative hystereris actually translate the lack of hysteresis in these conditions. Furthermore, the lack of secondary injection pressure investigated in the vicinity of this critical value does not allow to state whether the secondary injection location has an influence on the secondary mass flow rate ratio at which the local minimum occurs. Above this critical secondary mass flow rate ratio, the hysteresis starts to rise. In the present investigation, another decrease in hysteresis occured for the DBNi8 test specimen at a secondary mass flow rate ratio of 0.020. This second decrease was not observed with the other dual-bell nozzles. Figure 11 also shows that in the present investigation, the DBNi4 test specimen provides overall the largest hysteresis, with a maximum value of 18.8%, against 7% and 6.9% for the DBNi8 and DBN16 test specimen, respectively.

Previous studies^{5,6} showed the positive impact of secondary injection on side-loads generation in a subscale-dual-bell nozzle. The present investigation showed similar results, where a secondary mass flow rate ratio of less than 2% was sufficient to bring the side-loads generated during the transition and the retransition to less than 1% of the nozzle thrust (See Figure 12).

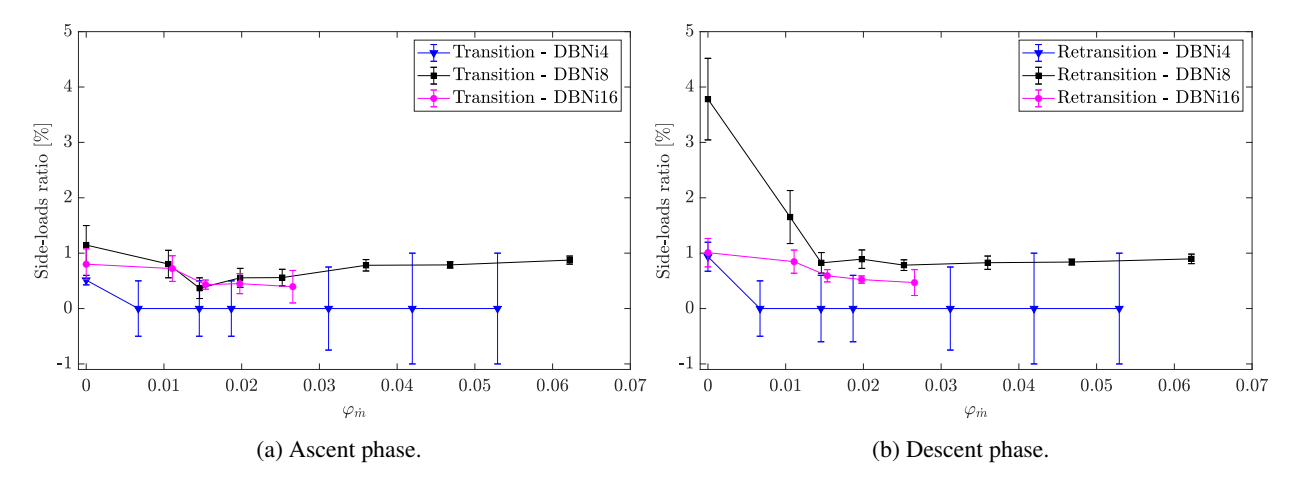


Figure 12: Side-loads ratio as a function of secondary mass flow rate ratio for different secondary injection positions.

4. Conclusions

This paper investigates the influence of the position of a transverse, annular secondary injection on the behaviour of a sub-scale dual-bell nozzle. Three nozzle configurations were tested, each featuring one secondary injection slot. The secondary injection slots were positioned at 4, 8, and 16 mm downstream of the inflection point. The nozzles were evaluated under varying secondary injection mass flow rate ratios and altitude conditions. Results were compared both across the different configurations and against a reference nozzle without secondary injection slot.

The experiments demonstrated that the mere presence of a secondary injection slot was sufficient to alter the nozzle's transition and retransition behaviour. The most pronounced effect was observed for the nozzle with the most upstream injection slot, where the transition nozzle pressure ratio increased by 19.2% compared to the reference. Conversely, the configuration with the furthest downstream slot exhibited a decrease in the transition pressure ratio by 0.07%, showcasing its limited influence during the ascent phases.

During the retransition phase, increases of 4.5% and 1.9% in the retransition pressure ratio were recorded for the configurations with injection slots at 4 mm and 8 mm, respectively. In contrast, the configuration with the furthest downstream injection slot led to a decrease of 3.7%.

For all configurations, the transition and retransition nozzle pressure ratios increased with the secondary mass flow rate ratio, up to a certain limit. These increases were capped at approximately 20-24% compared to the reference nozzle. Beyond a critical secondary mass flow rate ratio, a decline in both transition and retransition pressure ratios was observed for the 4 mm and 8 mm configurations, confirming trends reported in the authors' previous work. The

present investigation also showed that the peak effect occurred at lower seconday injection mass flow rates as the slot position moved upstream.

This decreasing trend was not observed for the most downstream configuration, where the transition and retransition occurred continuously, making it more difficult to identify clear transition and retransition nozzle pressure ratios. This change in transition behaviour represents a new result and offers an interesting direction for future investigation.

5. Acknowledgments

This document is the results of the research project funded by the grant no. ANR-22-ASTR-0037.

References

- [1] Swan Walter .C. The influence of nozzle design on the flight performance of rocket vehicles, with an analysis of the results of jet separation, 1948.
- [2] T Kimura, K Niu, K Yonezawa, and Y Tsujimoto. Experimental and analytical study for design of dual-bell nozzles. In 45th AIAA/ASME/SAE/ASEE Joint Propulsion Conference & Exhibit, 2009.
- [3] L. Leger, V. Zmijanovic, M. Sellam, and A. Chpoun. Controlled flow regime transition in a dual bell nozzle by secondary radial injection. *Experiments in Fluids*, 61, 12 2020.
- [4] L. Leger, V. Zmijanovic, M. Sellam, and A. Chpoun. Experimental investigation of forced flow regime transition in a dual bell nozzle by secondary fluidic injection. *International Journal of Heat and Fluid Flow*, 89, 6 2021.
- [5] Brian Legros. Flow control in dual-bell nozzles: optimisation of operating mode transition using radial secondary fluidic injection, April 2024.
- [6] Brian Legros, Luc Leger, Azeddine Kourta, Amer Chpoun, and Mohamed Sellam. Parametrical investigation of transverse injection in a dual-bell nozzle during altitude-varying conditions. *Journal of Propulsion and Power*, pages 1–11, 8 2023.
- [7] Emanuele Martelli, Francesco Nasuti, and Marcello Onofri. Numerical analysis of film cooling in advanced rocket nozzles. AIAA Journal, 47:2558–2566, 11 2009.
- [8] Francesco Nasuti, Marcello Onofri, and Emanuele Martelli. Role of wall shape on the transition in axisymmetric dual-bell nozzles. *Journal of Propulsion and Power*, 21:243–250, 2005.
- [9] Chloe Numberger-Genin and Ralf Stark. Experimental study on flow transition in dual bell nozzles. *Journal of Propulsion and Power*, 26(3):497–502, 2010.
- [10] Dzianis Proshchanka, Koichi Yonezawa, Hidekazu Koga, Yoshinobu Tsujimoto, Tatsuya Kimura, and Kazuhiko Yokota. Control of operation mode transition in dual-bell nozzles with film cooling. *Journal of Propulsion and Power*, 28:517–529, 2012.
- [11] Dirk Schneider, Ralf Stark, Chloé Génin, Michael Oschwald, and Konstantin Kostyrkin. Active control of dual-bell nozzle operation mode transition by film cooling and mixture ratio variation. *Journal of Propulsion and Power*, 36:47–58, 2019.
- [12] Takeo Tomita, Mamoru Takahashi, and Masaki Sasaki. Investigation on characteristics of conventional-nozzle-based altitude compensating nozzles by cold-flow tests (ii) side-load characteristics during transition. In 43rd AIAA/ASME/SAE/ASEE Joint Propulsion Conference & Exhibit. American Institute of Aeronautics and Astronautics, 7 2007.
- [13] Takeo Tomita, Mamoru Takahashi, and Masaki Sasaki. Control of transition between two working modes of a dual-bell nozzle by gas injection. In 45th AIAA/ASME/SAE/ASEE Joint Propulsion Conference & Exhibit, 2009.
- [14] Vladeta Zmijanovic. Secondary injection fluidic thrust vectoring of an axisymmetric supersonic nozzle. PhD thesis, Université d'Orléans,, 2013.
- [15] Vladeta Zmijanovic, Luc Leger, Mohamed Sellam, and Amer Chpoun. Assessment of transition regimes in a dual-bell nozzle and possibility of active fluidic control. *Aerospace Science and Technology*, 82-83:1–8, 11 2018.